Freak waves: beyond the Nonlinear Schrödinger breathers

Alessandro Iafrati[1], Alexander Babanin[2] and Miguel Onorato[3,4]

[1]*CNR-INSEAN - Italian Ship Model Basin - Roma, Italy;*
[2] *Swinburne Univ. Technology, Melbourne, Australia;*
[3]*Dip. di Fisica , Università di Torino, Via P. Giuria, 1 - Torino, 10125, Italy;*
[4] *INFN, Sezione di Torino, Via P. Giuria, 1 - Torino, 10125, Italy;*

ABSTRACT

Nowadays, it is well known that one of the mechanisms of formation of rogue or freak waves is the modulational instability. Usually this instability is studied in the framework of exact solutions of the Nonlinear Schrödinger equation, known as breathers. In the present paper we present a new approach to the problem and use the Direct Numerical Simulation (DNS) of the Navier-Stokes equation for a two-phase flow (water-air) to study the dynamics of the modulational instability and its effect on air and water. If the wave steepness of the initial wave is large enough we observe wave breaking and the the formation of large scale dipole structures in the air. Because of multiple steepening and breaking of the waves under unstable wave packets, a train of dipoles is released in the atmosphere at a height comparable with the wave length. The amount of energy dissipated by the breakers in water and air is considered and, contrary to expectations, we observe that energy dissipation in air is larger than the one in the water. Possible consequences on the exchange of aerosols, gasses and wave modelling is discussed.

1 Introduction

The modulational instability, also known as the Benjamin Feir instability in the ocean context, is a well known universal phenomenon that takes place in many different fields of physics such as surface gravity waves, plasma physics, nonlinear optics, see the recent historical review (Zakharov and Ostrovsky 2009). The basic idea consists in that a sufficiently steep sinusoidal wave may become unstable if perturbed by a long perturbation. It is a threshold mechanism, therefore, for example, for surface gravity waves in infinite water depth a wave is unstable if $2\sqrt{2}k_0A > K/k_0$, where k_0 is the wave number of the sinusoidal wave (carrier wave) and K is the wave number of the perturbation and A is the amplitude of the initial wave. It has been discovered in the sixties, but recently it has received again attention because it has been recognized that the modulational instability is a mechanism responsible for the formation of the rogue waves (Onorato et al. 2001; Janssen 2003). The main mathematical tool used to describe such physical phenomena is the Non Linear Schrördinger equation (NLS), which is a weakly nonlinear, narrow band approximation of the primitive equation of motions. The beauty of such equation is that it is integrable and many analytical solutions can be written explicitly. For example, breather solutions (Osborne et al. 2000; Dysthe and Trulsen 1999) have been considered as prototypes of rogue waves and have been observed in controlled experiments both in nonlinear optics, (Kibler et al. 2010), and water wave tank experiments (Chabchoub et al. 2011).

The studies on the modulational instability have been concentrated on the NLS dynamics and only more recently numerical computation of non-viscous potential fully nonlinear equations have been considered (Dyachenko and Zakharov 2008). Although rather efficient, the potential flow approach is no longer applicable once the instability develops. A first limit comes from the need of dealing with possible topological changes in the free surface. Furthermore, when the breaking occurs, vorticity is generated both by viscous effects and by the topological change of the interface in case of bubble entrainment processes. Moreover, so far none of the aforementioned literature have ever considered the effect of the

modulation instability on the fluid above and below the free surface. As far as we know this is the first paper in which the dynamics of air on water during the modulation process is investigated. This has been possible by simulating the Navier-Stokes equation for a two phase flow. This approach allows us to investigate conditions which are beyond the formal applicability of the NLS equation: for example, it is well known that if the initial wave steepness is large enough, the NLS equation is not able to describe the dynamics because the breaking of the wave takes place (Henderson et al. 1999). Breaking of surface waves, as an oceanic phenomenon (Babanin 2011), is important across a very broad range of applications related to wave dynamics, atmospheric boundary layer, air-sea-interactions, upper ocean turbulence mixing, with respective connections to the large-scale processes including ocean circulation, weather and climate (Cavaleri et al. 2012). Modulational instability and breaking has become also relevant in engineering applications such as naval architecture, structural design of offshore developments, marine transportation, navigation, among many others.

In the present work, the two-fluid flow of air and water is approximated as that of a single incompressible fluid whose density and viscosity vary smoothly across the interface and the Navier Stokes equations are solved. The paper is organized as follows: a brief review of the breather solutions of the NLS is reported in Section 2; in Section 3 a short description of the numerical method is presented and in Section 4 the implications of our numerical results are discussed.

2 Breathers solution of the Nonlinear Schrödinger equation

Starting from (Osborne et al. 2000) and (Dysthe and Trulsen 1999), breather solutions of the NLS equation have been considered as rogue wave prototypes. Here we give a quick overview of the Akhmediev solution (Akhmediev et al 1985; Akhmediev and Korneev 1986; Akhmediev et al 1987); it describes the modulational instability in its nonlinear regime; it is periodic in space. It is characterized by an amplification factor which ranges from 1 to 3 (this last value corresponds to the Peregrine solution). The breather has the following analytical form:

$$A(x,t) = A_0 \exp\left[-i\beta A_0^2 t\right] \left(\frac{\sqrt{2}\tilde{\nu}^2 \cosh[\Omega t] - i\sqrt{2}\tilde{\sigma}\sinh[\Omega t]]}{\sqrt{2}\cosh[\Omega t] - \sqrt{2-\tilde{\nu}^2}\cos[Kx]} - 1 \right) \tag{1}$$

and

$$\tilde{\nu} = \frac{K}{A_0}\sqrt{\frac{\alpha}{\beta}}, \quad \tilde{\sigma} = \tilde{\nu}\sqrt{2-\tilde{\nu}^2}, \quad \Omega = \beta A_0^2 \tilde{\sigma}, \tag{2}$$

K is the wave number of the perturbation and Ω corresponds to the exponential growth rate of the perturbation. The solution is periodic in space. The perturbation grows if $2 - \tilde{\nu}^2 > 0$, which for deep water waves corresponds to the condition $K < 2\sqrt{2}A_0 k_0^2$; not surprisingly such result corresponds to the standard one achieved by performing the linear stability analysis of a Stokes wave solution of the NLS equation. One can find the absolute maximum of the solution and, after some algebra, it is straightforward to show that

$$\frac{A_{max}}{A_0} = 1 + 2\sqrt{1 - \frac{\tilde{\nu}^2}{2}} = 1 + 2\sqrt{1 - \left(\frac{1}{2\sqrt{2}\varepsilon k_0/K}\right)^2}. \tag{3}$$

The maximum amplitude reached when $\varepsilon k_0/K \to \infty$; for such case A_{max}/A_0 is equal to 3, i.e. the Peregrine solution. In the water wave context, the steepness ε is alway less than one, therefore, in order to reach the limit one has to make a very long perturbation that includes a large number of waves under it. In figure 1 we show an example of such solution for steepness 0.1 and $k_0/K = 5$ with $A_{max}/A_0 = 2.4142...$.

It is straightforward to show that for large negative times, the solution (1) corresponds to $A_0 \exp(i\phi)(1 + \delta \cos(Kx))$ with $\delta \ll 1$. Recalling that the surface elevation is related to the envelope in the following

way:

$$\eta(x,t) = |A(x,t)|\cos(k_0 x - \omega_0 t), \tag{4}$$

the solution for the surface elevation at some initial time is:

$$\eta(x) = A_0 \cos(k_0 x) + \frac{1}{2}A_0 \delta \cos((k_0 + K)x) + \frac{1}{2}A_0 \delta \cos((k_0 - K)x) \tag{5}$$

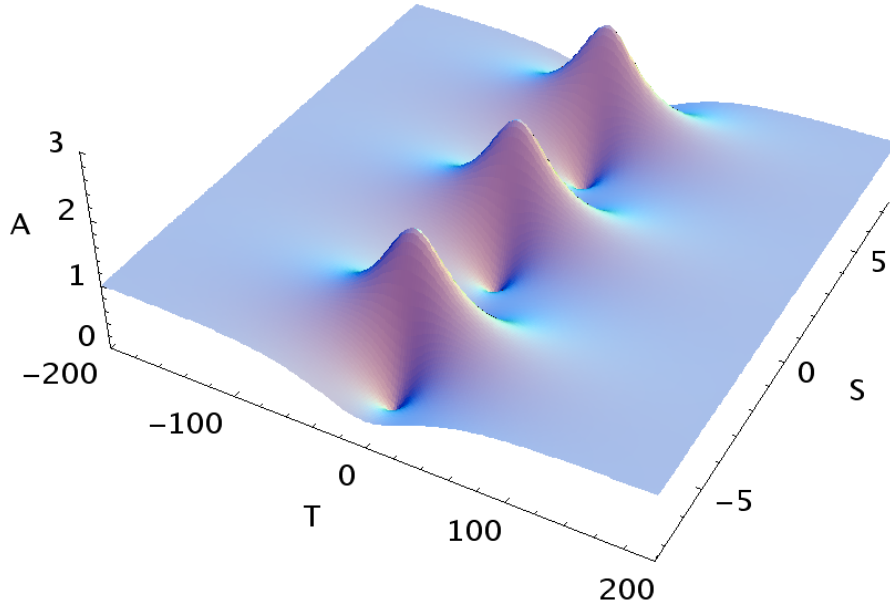This condition will be used for initializing the computation of the primitive equation of motion.

Figure 1: The Akhmediev solution: normalized wave envelope as a function of nondimensional time and space

3   The numerical method

The goal of the present section is to describe a numerical method for studying the evolution of the Akhmediev solution starting from the primitive equation of motion; the details of it can be found in (Iafrati 2010; Iafrati 2011), The continuity and momentum equations are written in generalized coordinates as follows:

$$\frac{\partial U_m}{\partial \xi_m} = 0 \ , \tag{6}$$

$$\frac{\partial}{\partial t}(J^{-1}u_i) + \frac{\partial}{\partial \xi_m}(U_m u_i) = -\frac{1}{\rho}\frac{\partial}{\partial \xi_m}\left(J^{-1}\frac{\partial \xi_m}{\partial x_i}p\right)$$

$$-J^{-1}\frac{\delta_{i2}}{Fr^2} - \frac{\kappa}{\rho\,We^2}\frac{\partial}{\partial \xi_m}\left(J^{-1}\frac{\partial \xi_m}{\partial x_i}H_{\delta_T}(d)\right)$$

$$+\frac{1}{\rho\,Re}\frac{\partial}{\partial \xi_m}\left(\mu G^{ml}\frac{\partial u_i}{\partial \xi_l} + \mu B^{mlji}\frac{\partial u_j}{\partial \xi_l}\right) \ . \tag{7}$$

In the above equations u_i is the i−th Cartesian velocity component, δ_{ij} is the Kronecker delta,

$$U_m = J^{-1} \frac{\partial \xi_m}{\partial x_j} u_j \qquad (8)$$

is the volume flux normal to the $\xi_m = const.$ surface and J^{-1} is the inverse of the Jacobian. Non-dimensional ratios are defined as

$$Fr = \frac{U_r}{\sqrt{gL_r}} \;,\; Re = \frac{U_r L_r \rho_w}{\mu_w} \;,\; We = U_r \sqrt{\frac{\rho_w L_r}{\sigma}}$$

for Froude, Reynolds and Weber numbers, respectively. Here, U_r and L_r are reference values for velocity and length, σ is the surface tension coefficient, ρ_w and μ_w are the values of the density and dynamic viscosity of water, respectively, which are also used as reference values for the corresponding quantities. In equation (7) G^{ml} and B^{mlji} are metric quantities and κ is the local curvature. The variation of the fluid properties and the surface tension forces is spread across a small neighborhood of the interface. This is done through a smoothed Heaviside function $H_\delta(d)$, where d is the signed distance from the interface, taken with the convention of a positive displacement being toward the water and negative displacement toward the air.

For the numerical solution, Cartesian velocities and pressure are defined at the cell centers, whereas volume fluxes are defined at the mid-point of the cell faces. The advancement in time is achieved through a fractional step approach in which the pressure contribution is neglected when integrating the momentum equation in time (*Predictor step*) and it is reintroduced in the next stage (*Corrector step*) when the continuity of the velocity field is enforced. In order to reduce the constraints of the related stability limit, the diagonal part of the first viscous contribution in (7) is computed implicitly with a Crank-Nicholson scheme, whereas all other terms are computed explicitly with a three-steps low storage Runge-Kutta scheme.

The pressure corrector, is found by enforcing the continuity of the velocity field at the end of the substep. This gives rise to a Poisson equation

$$\frac{\partial}{\partial \xi_m} \left(\frac{G^{mj}}{\tilde{\rho}^l} \frac{\partial \tilde{\Phi}^l}{\partial \xi_j} \right) = \frac{1}{\Delta t} \frac{\partial \hat{U}_m^l}{\partial \xi_m} -$$
$$\frac{\zeta_{l-1}}{\gamma_l} \frac{\partial}{\partial \xi_m} \left(\frac{G^{mj}}{\tilde{\rho}^{l-1}} \frac{\partial \tilde{\Phi}^{l-1}}{\partial \xi_j} \right) \;. \qquad (9)$$

where the apex l denotes the substep index of the third order Runge-Kutta scheme, and ζ, γ are time advancing coefficients. The Poisson equation is solved by using a BiCGStab algorithm, in combination with an Incomplete LU decomposition for the preconditioning.

The interface between air and water is captured as the zero level-set of a signed normal distance from the interface $d(\boldsymbol{x}, t)$ which, at $t = 0$, is initialized by assuming $d > 0$ in water, $d < 0$ in air. Physical fluid properties are assumed to be related to d by the equation:

$$f(d) = f_a + (f_w - f_a) H_\delta(d) \qquad (10)$$

where the parameter δ is chosen so that the density and viscosity jumps are spread across five grid cells, at least, see (Iafrati and Campana 2005). The distance function is advected in time with the flow as a non-diffusive scalar by using the equation

$$\frac{\partial d}{\partial t} + \boldsymbol{u} \cdot \nabla d = 0 \;. \qquad (11)$$

The integration in time of the above equation is carried out with the same three-steps Runge-Kutta and discretization scheme employed for the convective terms. At the end of each time step, the interface

location is identified as the zero level of the updated field $d(\boldsymbol{x},t)$. Because the function d is defined at the cell centers, in discrete form the interface is reconstructed onto the staggered grid as a set of segments which are identified by taking the intersection of the $d = 0$ level with the bilinear interpolation of the values the function d takes at the four nodes of the cell. Although this choice implies that the interface reconstruction is only first order accurate in space, it allows the identification of interface portion within one cell without involving the values the function d takes at the nodes of the contiguous cells, thus making the reconstruction procedure very simple even in presence of complex interface topologies.

In order to keep the width of the jump region separating the two fluids constant through time, the function d is reinitialized by computing the minimum distance from the new interface configuration to the cell centers, after the new free surface shape is reconstructed. It is worth remarking that, to avoid changing the interface location throughout the reconstruction process, the distance function is not reinitialized on the nodes belonging to cells crossed by the interface.

4   Computation of the modulational instability

In our simulations we consider the standard modulational instability process as the one for example produced in the experimental work in (Tulin and Waseda 1999) (see also equation (2)). The initial surface elevation consists in a sinusoidal perturbed wave (see (2))

$$\eta(x,t=0) = A_0\cos(k_0 x) + A_1\cos((k_0+K)x) + A_1\cos((k_0-Kx)) \tag{12}$$

where k_0 is the wavenumber of the fundamental component and K is the wavenumber of the perturbation. In the simulations presented in the following $\varepsilon_0 = k_0 A_0$ is varied from 0.1 to 0.18, with a step 0.02. Such conditions corresponds to the early stages of an Akhmediev breather (Akhmediev et al 1987). Because of the typical time scale of the modulational instability is of the order of 100 periods, the Navier-Stokes simulation is expensive and for the initial development of the instability a standard potential code is used. The sideband components are at $K = k_0/5$ and their amplitude is $A_1 = 0.1A_0$. The simulation is initialized with velocities in air and water corresponding to the analytical solution for linear potential flow. For convenience, results are presented in dimensional form. Simulations are carried out for a fundamental component with $\lambda_0 = 0.60$ m, with $g = 9.81$ m s^{-1}. The computational domain which spans horizontally from x = -1.5 m to x = 1.5 m and vertically from y= -2 m up to 0.6 m above the still water level. The domain is uniformly discretized in the horizontal direction with Δx = 1/1024 m. Vertically, the grid spacing is uniform, and equal to Δx, from y = -0.15 to 0.15 m whereas it grows geometrically by a factor α= 1.03 towards the upper and lower boundaries. This gives a total of 3072 $\times$ 672 grid cells The total thickness of the transition region is 0.01 m, so that the density jump is spread across about 10 grid cells. Although neglected in the potential flow model, surface tension effects are considered in the Navier-Stokes solution for which the surface tension coefficient is assumed to be that in standard conditions $\sigma = 0.073$ N m^{-1}. In the two-fluid modelling, the densities of air and water are the standard ones, $\rho_w = 1000$ kg m^{-3} and $\rho_a = 1.25$ kg m^{-3}. The values of the dynamic viscosities in water and air are $\mu_w = 10^{-3}$ kg m^{-1} s^{-1} and $\mu_a = 1.8\,10^{-5}$ kg m^{-1} s^{-1}, respectively.

Because of the large computational time needed for the computation of the NS equation, the wave field is evolved using a fully nonlinear potential code and as breaking is approached the NS solver is used. As expected, the process observed in the simulation corresponds to the standard modulational instability (exponential growth of the side bands) up to the point where the wave group reaches its strongly nonlinear regime and eventually wave breaking is observed. In figure 2 an example for steepness k_0A_0=0.18 of the simulation of the wave breaking resulting from the modulational instability is shown; the formation of a first jet is observed which entrap air. The jet then bounces on the free surface creating a second air bubble. Some droplets of water in air are also visible; a small amount of vorticity is also released close to the surface.
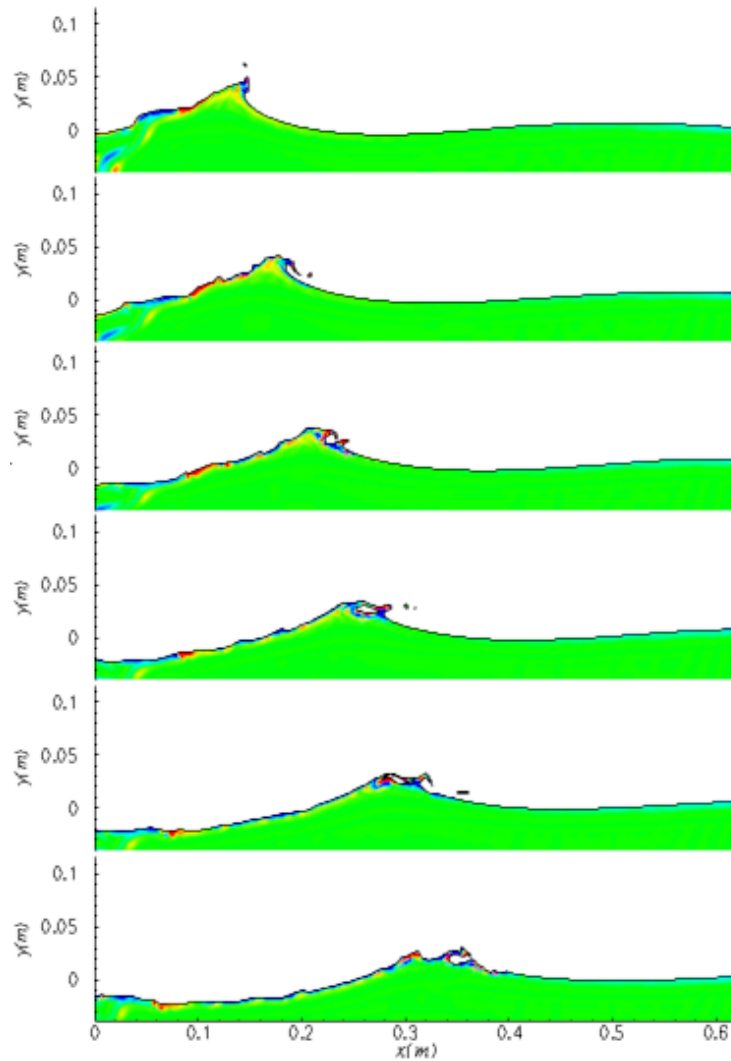
Figure 2: Breaking event for initial steepness $\varepsilon_0=0.18$. The color corresponds to the vorticity field: green corresponds to zero vorticity, blue to -20 sec^{-1} and red to 20 sec^{-1}. The Δt between each image is 0.05 sec.
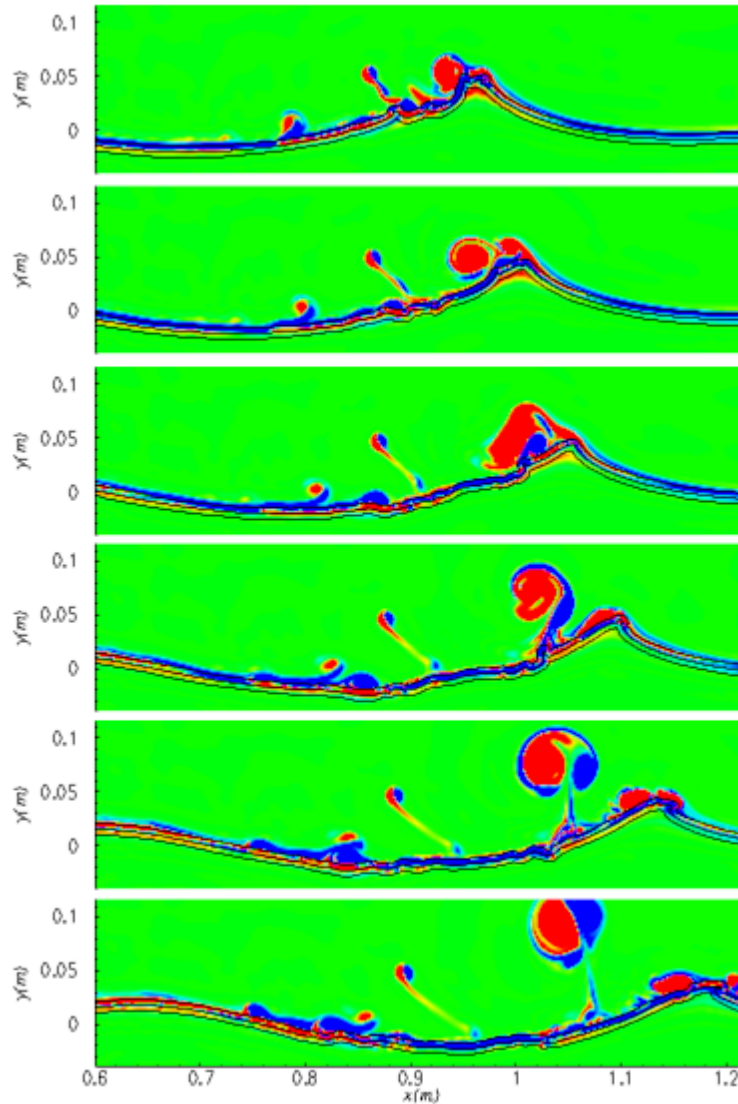
Figure 3: Sequence of formation of a dipole in air as a consequence of the wave breaking. The Δt between each image is 0.05 sec. The initial steepness is 0.18

It is of particular interest to focus the attention on the dynamic of the air flow. In figure 3 we show a sequence of snap-shots of the water and air domain where the roll-up of a dipole structure is observed for initial steepness of 0.16: the fast steepening of the wave profile and the wave breaking causes the air flow to separate from the crest giving rise to a large, positive, vorticity structure (positive vorticity is in red). The interaction of this vortex structure with the free surface leads to the formation of a secondary vorticity structure of opposite sign, which eventually detaches from the free surface and forms a dipole which moves under the self-induced velocity. It should be stressed that such phenomenon is not observed if the wave breaking process does not take place: we have performed a numerical simulation with $\varepsilon = 0.1$ which does not lead to a breaking event and no evident dipole structures are observed. The group velocity is half the phase velocity, therefore each single wave that passes below the group (at its maximum height), breaks. The result is that a series of dipoles are released in the atmosphere as shown in figure 4 where the a strip of the computational domain is shown. Vortices of various sizes and dipoles are clearly observable in the domain. Two things should be noted: i) the height of the highest dipoles is of the order of the wavelength; ii) large amount of vorticity is observed in the air and not in the water. One major question to be answered, especially in the spirit of modelling the dissipation term in the wave
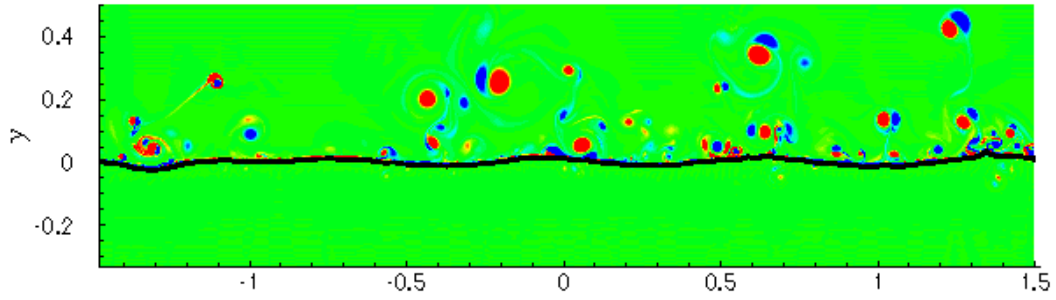
Figure 4: *Vorticity field in a portion of the computational domain close to the surface.The scale of vorticity is as described in the label of figure 2. The initial steepness is 0.18*
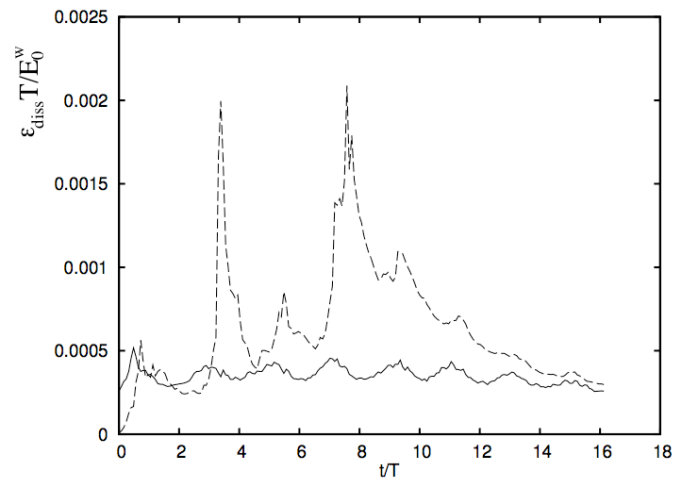

Figure 5: *Dissipation nondimensionalized with period T and total energy in the water, E_0^w a t = 0 as a function of nondimensional time for water (solid line) and air (dashed line). The initial steepness is 0.12*

Figure 6: *Dissipation nondimensionalized with period T and total energy in the water, E_0^w a t = 0 as a function of nondimensional time for water (solid line) and air (dashed line). The initial steepness is 0.18*
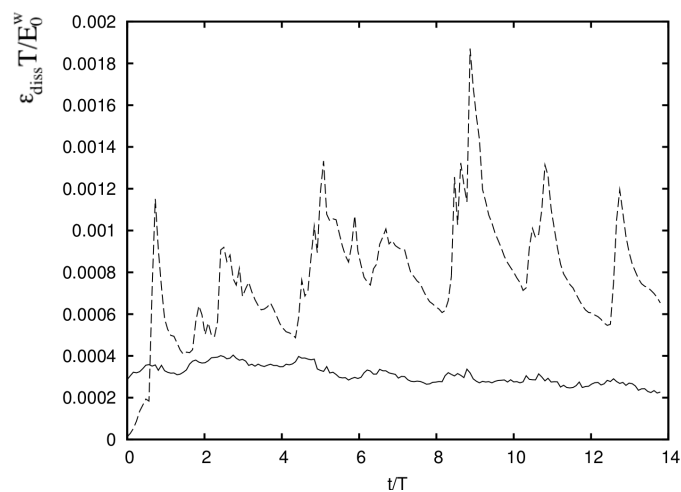
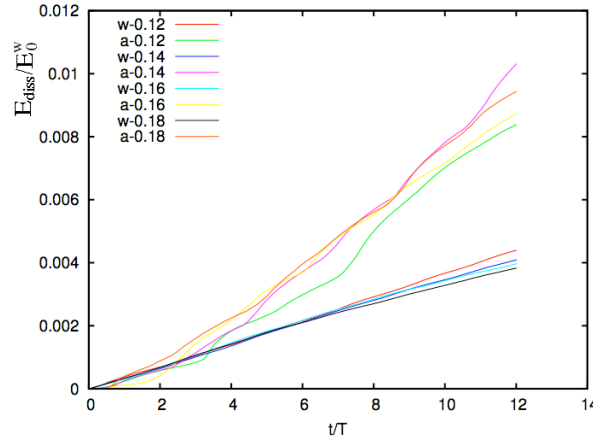*Figure 7: Integrated dissipation for different values of the steepness in water (w) and air (a).*

forecasting models ([Komen et al. 1994](#)), is the amount of energy dissipated during a wave breaking or a sequence of breaking events. Therefore, a quantitative estimate of the dissipated energy both in air and water can can be obtained by integrating the viscous stresses over the air and water domain:

$$\varepsilon_{diss}^{w}(t) = \int_{d \geq 0} 2\mu e_{ij} \frac{\partial u_i}{\partial x_j} dx dy \qquad (13)$$

$$\varepsilon_{diss}^{a}(t) = \int_{d < 0} 2\mu e_{ij} \frac{\partial u_i}{\partial x_j} dx dy \qquad (14)$$

where e_{ij} is the symmetric part of the strain tensor. In figure 5 and 6 we show the dissipation function normalized by the initial energy of the water and wave period, T, as a function of time nodimensionalized by T for two simulations with steepness $\varepsilon = 0.12$ and $\varepsilon = 0.18$ respectively; the origin of the time axis is set to the time at which the Navier Stokes simulations takes over the simulation with the potential code. The occurrence of spikes in the energy content in air indicates that an energy fraction is transferred to air and is successively dissipated by the viscous stresses. The multiple peaks correspond to the multiple breaking that occurs during the modulational instability process (as mentioned before, the group is slower than the phase velocity and each wave breaks as it passes below it). Similar plots are observed for larger steepness.

In order to show how relevant is the energy dissipation in the air in comparison to the corresponding one in water consider the following integrated quantity:

$$E_{diss}(t) = \int_0^t \varepsilon_{diss}(t') dt'. \qquad (15)$$

The integral is considered in water and air. Histories of the integrals in time of the viscous dissipation terms in the two media are shown. It is rather interesting to see that, in nondimensional form, the solutions for the four different cases are almost overlapped to each other, with a total dissipation in air about three times that in water.

5   Discussion and conclusion

Modulated waves of different initial steepnesses starting from 0.12 have been analyzed using the two phase flow NS equation. In all cases, a first breaking event has been found shortly after the start of the two-fluids model and successive events have been found with a period about two times the period of the fundamental wave component. Spray is the natural consequence of the wave breaking. Very

small droplets of water are thrown in the air. Some of these particles are so tiny (aerosols) that they can remain in the air for a very long time, forming condensation nuclei for clouds and affecting incoming solar radiation. Our simulations show that vortices rise up to the height of the wave lengths and can in principle transport aerosols (not resolved in our simulations). Aerosols may have different implications. Besides being the base for cloud condensation nuclei, they scatter electromagnetic radiation and reflect solar radiation. Rather interesting, an intense flow has been found to be induced in air as a consequence of the fast steepening and breaking process. Quantitative analyses of the energy contents and of the viscous dissipation term have been provided. Even bearing in mind the limits of the numerical model, the results indicate that, due to the highly rotational flow in air, the dissipation of the energy during the multiple breaking of modulationally unstable wave is mostly concentrated in the air side.

The present work represents the first attempt to approach the problem of modulational instability starting from the Navier-Stokes equation. Results seems to be very encouraging. Clearly, it has a number of limitation due to the heaviness of the computation. Probably the most important one is that we have assumed that waves are long crested and the fluid domain is 2-dimensional. In reality, we expect that 3D effect can take place and dipoles and vortices can become unstable. It will be just a matter of time to develop the 3D version of the NS code and verify our finding in a more realistic context. A second important limitation is the lack of wind: our simulations correspond to the propagation of a steep swell and what would be the consequences of a turbulent wind on the generation of vorticity during breaking event is unknown.

Acknowledgements

References

Akhmediev, N., V. Eleonskii, and N. Kulagin (1985). Generation of periodic trains of picosecond pulses in an optical fiber: exact solutions. *Sov. Phys. JETP 62*(5), 894–899.

Akhmediev, N., V. Eleonskii, and N. Kulagin (1987). Exact first-order solutions of the nonlinear Schr "odinger equation. *Theoretical and Mathematical Physics 72*(2), 809–818.

Akhmediev, N. and V. Korneev (1986). Modulation instability and periodic solutions of the nonlinear schrödinger equation. *Theoretical and Mathematical Physics 69*(2), 1089–1093.

Babanin, A. (2011). *Breaking and dissipation of ocean surface waves*. Cambridge Univ Pr.

Cavaleri, L., B. Fox-Kemper, and M. Hemer (2012). Wind waves in the coupled climate system. *Bulletin of the American Meteorological Society, Accepted for pubblication.*

Chabchoub, A., N. Hoffmann, and N. Akhmediev (2011). Rogue wave observation in a water wave tank. *Physical Review Letters 106*(20), 204502.

Dyachenko, A. and V. Zakharov (2008). On the formation of freak waves on the surface of deep water. *JETP letters 88*(5), 307–311.

Dysthe, K. B. and K. Trulsen (1999). Note on breather type solutions of the nls as models for freakwaves. *Physica Scripta T82*, 48–52.

Henderson, K., D. Peregrine, and J. Dold (1999). Unsteady water wave modulations: fully nonlinear solutions and comparison with the nonlinear schrödinger equation. *Wave Motion 29*(4), 341–361.

Iafrati, A. (2010). Numerical study of the effects of the breaking intensity on wave breaking flows. *Journal of Fluid Mechanics 622*, 371.

Iafrati, A. (2011). Energy dissipation mechanisms in wave breaking processes: Spilling and highly aerated plunging breaking events. *Journal of Geophysical Research 116*(C7), C07024.

Iafrati, A. and E. Campana (2005). Free-surface fluctuations behind microbreakers: space-time behaviour and subsurface flow field. *Journal of Fluid Mechanics 529*, 311–347.

Janssen, P. A. E. M. (2003). Nonlinear four–wave interaction and freak waves. *J. Phys. Ocean. 33*(4), 863–884.

Kibler, B., J. Fatome, C. Finot, G. Millot, F. Dias, G. Genty, N. Akhmediev, and J. Dudley (2010). The Peregrine soliton in nonlinear fibre optics. *Nature Physics 6*(10), 790–795.

Komen, G., L. Cavaleri, M. Donelan, K. Hasselmann, H. Hasselmann, and P. Janssen (1994). *Dynamics and modeling of ocean waves*. Cambridge: Cambridge University Press.

Onorato, M., A. Osborne, M. Serio, and S. Bertone (2001). Freak wave in random oceanic sea states. *Phys. Rev. Lett. 86*(25), 5831–5834.

Osborne, A., M. Onorato, and M. Serio (2000). The nonlinear dynamics of rogue waves and holes in deep–water gravity wave train. *Phys. Lett. A 275*, 386–393.

Song, J. and M. Banner (2002). On determining the onset and strength of breaking for deep water waves. part i: Unforced irrotational wave groups. *J. Phys. Ocean. 32*, 2541–2558.

Tulin, M. P. and T. Waseda (1999). Laboratory observation of wave group evolution, including breaking effects. *J. Fluid Mech. 378*, 197–232.

Zakharov, V. and L. Ostrovsky (2009). Modulation instability: the beginning. *Physica D: Nonlinear Phenomena 238*(5), 540–548.